Electrostatic electron cyclotron harmonic instability due to energetic electrons in Jupiter's magnetosphere

A. K. Tripathi and R. P. Singhal

Department of Applied Physics, Institute of Technology, Banaras Hindu University, Varanasi, India

Received 1 March 2005; revised 27 June 2005; accepted 14 September 2005; published 3 December 2005.

[1] Electrostatic electron cyclotron harmonic instability in the magnetosphere of Jupiter is investigated using a kappa distribution with loss cone for energetic electrons in the tail of the distribution function. Temporal growth rates are calculated at two representative radial distances characterized by different temperatures of the thermal electron population. It is found that the frequency within the harmonic band shifts to a lower value as the temperature of the thermal electron population increases. Furthermore, higher harmonic bands are damped faster as the angle between the wave normal and the ambient magnetic field is decreased. Calculations are performed by changing various parameters appearing in the distribution function. The present study may be helpful in accounting for some of the observed features of the electron cyclotron harmonic bands in the magnetosphere of Jupiter. The observed features are as follows: (1) Maximum amplitudes are usually seen in the first harmonic band and at the highest frequency of emission near upper hybrid resonance, (2) Emissions are greatest at smaller radial distances and decrease with increasing distance, (3) The amplitude is observed to fluctuate over more than an order of magnitude on timescales of several seconds.

Citation: Tripathi, A. K., and R. P. Singhal (2005), Electrostatic electron cyclotron harmonic instability due to energetic electrons in Jupiter's magnetosphere, *J. Geophys. Res.*, *110*, A12205, doi:10.1029/2005JA011113.

1. Introduction

[2] Voyager encounters with Jupiter have provided us with the first comprehensive investigation of plasma waves in the magnetosphere of Jupiter. The most striking feature of the Jovian plasma wave observations is the very close similarity to the plasma wave phenomena observed in the Earth's magnetosphere. Plasma waves observed in Jupiter's magnetosphere include electrostatic waves near and upstream of the bow shock, electromagnetic continuum radiation, whistler mode chorus and hiss, electrostatic electron cyclotron and upper hybrid emissions, and broadband electrostatic noise [*Scarf et al.*, 1981; *Gurnett and Scarf*, 1983; *Kurth and Gurnett*, 1991; *Zarka*, 2004]. Pioneer and Voyager encounters with Jupiter have also resulted in a dramatic increase in our detailed knowledge of the plasma properties of the Jovian magnetosphere [*Bridge et al.*, 1979a, 1979b; *Belcher*, 1983]. The Ulysses encounter with Jupiter has produced new observations of the Jupiter environment [*Bird et al.*, 1992; *Stone et al.*, 1992]. More recently, Galileo spacecraft explored the Jovian system and provided new data on plasma waves in the Io plasma torus and near Io. The Galileo plasma wave instrument detected narrowband upper hybrid waves during the inbound pass through the Io torus. It was found that the electron density in the torus increased by about a factor of 2 since the Voyager 1 flyby [*Gurnett et al.*, 1996a].

0148-0227/05/2005JA011113

[3] Inside of about 23 R_J, electron cyclotron harmonic (ECH) emissions are the main features of the inner Jovian magnetosphere and are extremely well confined to the Jovian magnetic equator. The cyclotron emissions extend from just above the local electron gyrofrequency (f_{ce}) to the upper hybrid resonance frequency (f_{UHR}). The intensity of the ECH bands at Jupiter is typically 100 μV/m with occasional bursts to few millivolts per meter. During an individual event the amplitude is observed to fluctuate over more than an order of magnitude on timescales of several seconds. Maximum amplitudes are usually seen in the band just above f_{ce} and at the highest frequency of emission near f_{UHR}. The intensities of the emissions are greatest at smaller radial distances and decrease with increasing distance [*Kurth et al.*, 1980; *Gurnett and Scarf*, 1983; *Kurth*, 1992]. During the Ulysses encounter with Jupiter, intense emissions were recorded near 3/2 f_{ce} and 5/2 f_{ce} when the spacecraft crossed the magnetic equator in the Io torus [*Stone et al.*, 1992]. Narrowband electrostatic emissions are also observed by the Galileo plasma wave instrument during the inbound pass through the Io torus [*Gurnett et al.*, 1996a]. The Galileo spacecraft executed nine close flybys of Jupiter's moon Europa and four close flybys of Ganymede, for which plasma wave observations were obtained [*Gurnett et al.*, 1996a, 1996b; *Kurth et al.*, 2001]. On the upstream side of Europa, electron cyclotron harmonics are observed. These emissions are driven by loss and production of plasma at Europa as a result of the interaction of the Jovian magnetosphere with the moon. Detection of electrostatic electron cyclotron and other types of waves around Gany-

mede suggest that the moon has a large, extended magnetosphere of its own.

[4] In the present study we investigate the growth rates of the electrostatic ECH bands in the magnetosphere of Jupiter. Within the Jovian magnetosphere these emissions were detected over a wide range of radial distances [*Kurth et al.*, 1980; *Stone et al.*, 1992; *Gurnett et al.*, 1996a]. On the basis of similar observations in the Earth's magnetosphere these emissions are identified as electron cyclotron waves near half-integral harmonics of the electron cyclotron frequency $(n + \frac{1}{2})f_{ce}$. The intensities of these waves vary over a wide range, from only a few microvolts per meter to a few millivolts per meter [*Kurth et al.*, 1980]. The identification of a given emission band with a specific half-integral harmonic is only an identifying name and does not necessarily imply that the emission frequency is exactly at the half-integral harmonic. The detailed growth rate of the electrostatic instability and the number of unstable bands depend on a large number of parameters, the most important of which are the cold-to-hot electron concentration ratio and the cold and hot electron temperature. The study of electron cyclotron harmonics in the Jovian magnetosphere is important for several reasons. (1) If the waves are sufficiently intense, they can cause pitch angle diffusion and loss of energetic electrons trapped in the magnetic field and subsequent precipitation into the atmosphere. (2) These waves can energize the cold electron population.

[5] Electron distribution functions measured in the inner magnetosphere of Jupiter show a well-developed thermal population that is well fit by Maxwellian distribution and also show a distinct suprathermal tail [*Belcher*, 1983]. The low-density suprathermal population is a free energy source for ECH waves. The suprathermal tail is modeled by kappa distribution [*Divine and Garrett*, 1983; *Summers and Thorne*, 1992, 1995; *Collier*, 2004], which joins smoothly into the thermal population. Suprathermal electrons described by a kappa distribution have been used to explain whistler instability in the magnetospheres of Earth and Jupiter [*Leubner*, 1982; *Mace*, 1998]. Electrostatic electron cyclotron (Bernstein) waves have been studied in the magnetosphere of Jupiter using a power law distribution for suprathermal electrons [*Barbosa and Kurth*, 1980].

[6] In the present work we invoke the kappa distribution with loss cone feature to study the electrostatic ECH (Bernstein) emissions in the magnetosphere of Jupiter. In section 2 we describe the dispersion relations and expression for growth of instability using a kappa loss cone distribution. In section 3, plasma parameters appropriate for the magnetosphere of Jupiter and used in the present analysis are discussed. Section 4 contains the results. Discussion and conclusions of the present work are given in section 5.

2. Dispersion and Growth of Instability

[7] We consider the plasma to be immersed in a uniform magnetic field $\mathbf{B} = B_0\hat{e}_z$, and all configuration space gradients of the plasma are considered to vanish. We are interested in high-frequency waves such that $\omega > \Omega_c$, where Ω_c is the electron gyrofrequency; hence we neglect ion dynamics. For the electrostatic modes the dispersion equation is written as [*Clemmow and Dougherty*, 1969]

$$D(\mathbf{k},\omega) = 1 + \sum_{\alpha} 2\pi\frac{\omega_{p\alpha}^2}{k^2}\int_{-\infty}^{\infty} dv_{\parallel}\int_{0}^{\infty} dv_{\perp} v_{\perp} \cdot \sum_{n=-\infty}^{\infty}\frac{J_n^2(k_{\perp}v_{\perp}/\Omega_{\alpha})}{\omega - n\Omega_{\alpha} - k_{\parallel}v_{\parallel}}\left(\frac{n\Omega_{\alpha}}{v_{\perp}}\frac{\partial}{\partial v_{\perp}} + \mathrm{k}_{\parallel}\frac{\partial}{\partial v_{\parallel}}\right) f_{\alpha} = 0, \tag{1}$$

where $\alpha = c, h$ for the thermal and energetic electron components, respectively, $\mathbf{k} = k\hat{e}_z + k_{\perp}$ is the wave propagation vector, and $\mathbf{v} = v_{\parallel}\hat{e}_z + \mathbf{v}_{\perp}$ is the velocity. We define $\omega_{p\alpha}^2 = 4\pi n_{\alpha} q_{\alpha}^2/m_{\alpha}$ for species α with mass m_{α}, charge q_{α}, and number density n_{α}, and $\Omega_{\alpha} = |q_{\alpha}|B_0/m_{\alpha}c$. J_n are the Bessel functions [*Abramowtiz and Stegun*, 1970].

[8] Defining $\omega = \omega_r + i\gamma$, where $\omega_r = \mathrm{Re}(\omega)$ is the real frequency and $\gamma = \mathrm{Im}(\omega)$ is the growth rate with $\gamma > 0$ corresponding to instability, equation (1) can be expressed as

$$D(\mathbf{k}, \omega_r + i\gamma) = 0. \tag{2}$$

Defining $D_r = \mathrm{Re}(D)$ and $D_i = \mathrm{Im}(D)$ and Taylor series expansion $D = D_r + iD_i = 0$ for weak instability (small γ and D_i), we obtain

$$D_r(\mathbf{k}, \omega_r) = 0 \tag{3}$$

$$\gamma = -\frac{D_i(\mathbf{k}, \omega_r)}{\partial D_r(\mathbf{k}, \omega_r)/\partial\omega_r}. \tag{4}$$

D_i can be obtained from equation (1) making use of

$$\frac{1}{\omega_r - n\Omega_{\alpha} - k_{\parallel}v_{\parallel} + i\gamma} = P\frac{1}{\omega_r - n\Omega_{\alpha} - k_{\parallel}v_{\parallel}} - i\pi\delta\left(\omega_{\mathrm{r}} - n\Omega_{\alpha} - k_{\parallel}v_{\parallel}\right), \tag{5}$$

where P denotes the Cauchy principal value and δ is the Dirac delta function [*Mathews and Walker*, 1965].

[9] We consider a plasma where the entire electron distribution function is the superposition of a kappa distribution with loss cone f_k, introduced by *Summers and Thorne* [1991, 1995] (ST model), representing the low-density tail population and a Maxwellian distribution for thermal component f_M given by

$$f_M = \frac{1}{\pi^{3/2}v_{c_{\perp}}^2 v_{c_{\parallel}}}\exp\left(-v_{\perp}^2/v_{c_{\perp}}^2 - v_{\parallel}^2/v_{c_{\parallel}}^2\right), \tag{6}$$

where

$$v_{c_{\perp,\parallel}}^2 = 2T_{c_{\perp,\parallel}}/m_e \tag{7}$$

$$f_{\kappa} = \frac{1}{\pi^{3/2}\theta_{\perp}^2\theta_{\parallel}}\frac{\Gamma(\kappa+\ell+1)}{\kappa^{\ell+3/2}\Gamma(\ell+1)\Gamma(\kappa-1/2)}\left(\frac{v_{\perp}}{\theta_{\perp}}\right)^{2\ell} \cdot\left(1 + \frac{v_{\parallel}^2}{\kappa\theta_{\parallel}^2} + \frac{v_{\perp}^2}{\kappa\theta_{\perp}^2}\right)^{-(\kappa+\ell+1)}, \tag{8}$$

where

$$\theta_\perp = \left(\frac{2\kappa-3}{\kappa}\right)^{1/2}(\ell+1)^{-1/2}(T_{h_\perp}/m_e)^{1/2} \quad (9)$$

$$\theta_\parallel = \left(\frac{2\kappa-3}{\kappa}\right)^{1/2}\left(T_{h_\parallel}/m_e\right)^{1/2}. \quad (10)$$

Γ is the gamma function. The parameter ℓ (>0) is the "loss cone index," and the parameter κ (>3/2) is the "spectral index"; ℓ is a measure of the angular size of the effective loss cone region ($\partial f_\kappa/\partial v_\perp > 0$), and κ is a measure of the relative number of particles in the high-energy tail of the distribution. The distribution function has been normalized to 1. $T_\parallel$ and $T_\perp$ are the parallel and perpendicular temperature, respectively, of each species α given by

$$T_{\perp\alpha} = \frac{1}{2}m_\alpha \int v_\perp^2 f_\alpha d^3v \quad (11)$$

$$T_{\parallel\alpha} = m_\alpha \int v_\parallel^2 f_\alpha d^3v, \quad (12)$$

where $\theta_\parallel$ and $\theta_\perp$ are the parallel and perpendicular effective thermal speeds, respectively. More recently, *Leubner and Schupfer* [2001] (LS model) and *Leubner* [2004] have introduced a kappa loss cone distribution applicable to a variety of space plasma modeling

$$f_\kappa = \frac{1}{\pi^{3/2}v_{th_\perp}^2 v_{th_\parallel}} \frac{\Gamma(\kappa+1)}{\kappa^{\ell+3/2}\Gamma(\ell+1)\Gamma(\kappa-\ell-1/2)}\left(\frac{v_\perp}{v_{th_\perp}}\right)^{2\ell} \cdot \left(1+\frac{v_\parallel^2}{\kappa v_{th_\parallel}^2}+\frac{v_\perp^2}{\kappa v_{th_\perp}^2}\right)^{-(\kappa+1)}, \quad (13)$$

where

$$v_{th_{\parallel,\perp}} = \left(2T_{\parallel,\perp}/m_e\right)^{1/2}. \quad (14)$$

It may be noted that in equation (13), $\kappa - \ell - 1/2 > 0$ is a profound constraint. Using the distribution function equation (8) results in a decreased effective temperature for any finite value of kappa (for loss cone index $\ell = 0$), while equation (13) gives effective temperatures, which are increased for finite values of κ. We further assume that $T_c = T_{c_\perp} = T_{c_\parallel}$ and $T_h = T_{h_\perp} = T_{h_\parallel}$. Since $n_c \gg n_h$, the real part of the frequency ω_r will be determined by the Maxwellian distribution. The dispersion equation for ω_r becomes

$$1 = \frac{2\omega_{pc}^2}{\lambda}\sum_{n=1}^{\infty} e^{-\lambda}I_n(\lambda)\frac{n^2}{\omega_r^2 - n^2\Omega_c^2} + \omega_r\omega_{pc}^2\cos^2\psi e^{-\lambda} \cdot \sum_{n=-\infty}^{\infty} I_n(\lambda)\frac{1}{(\omega_r - n\Omega_c)^3}, \quad (15)$$

where ψ is the angle between **k** and **B** and $I_n(\lambda)$ are modified Bessel functions [*Abramowtiz and Stegun*, 1970] with

$$\lambda = \frac{T_c k^2}{m_e\Omega_c^2}. \quad (16)$$

[10] Equation (15) is written for $k_\parallel \ll k_\perp$. The second term on the right-hand side is the small correction for finite $k_\parallel$. The ratio of the correction term to the first main term in equation (15) is given by $k^2\, v_c^2\cos^2\psi/2(\omega_r - n\Omega_c)^2 = v_c^2/2v_R^2$. Using equation (5), the imaginary part of dispersion D_i for isotropic Maxwellian distribution is obtained as

$$D_i^M = \sum_{n=-\infty}^{\infty}\frac{2\pi^{1/2}\omega_{pc}^2\omega}{k^2k_\parallel v_c^3}\exp\left(-\frac{v_R^2}{v_c^2}\right)e^{-\lambda}I_n(\lambda), \quad (17)$$

where v_R is the resonant velocity given by

$$v_R = \frac{\omega_r - n\Omega_c}{k_\parallel}. \quad (18)$$

The imaginary part of dispersion equation for kappa distribution equation (8) is written as

$$D_i^\kappa - = -\frac{2\pi^2\omega_{ph}^2}{k^2k_\parallel}\sum_{n=-\infty}^{\infty}\left[2\ell an\Omega_c g_1 - 2a(\kappa+\ell+1)\frac{n\Omega_c}{\kappa\theta_\perp^2}g_2 - 2a(\kappa+\ell+1)\frac{k_\parallel v_R}{\kappa\theta_\parallel^2}g_2\right], \quad (19)$$

where

$$a = \frac{\Gamma(\kappa+\ell+1)}{\pi^{3/2}\theta_\perp^2\theta_\parallel\kappa^{\ell+3/2}\Gamma(\ell+1)\Gamma(\kappa-1/2)(\theta_\perp)^{2\ell}}, \quad (20)$$

$$g_1 = (b)^{2\ell}\left(1+\frac{v_R^2}{\kappa\theta_\parallel^2}\right)^{-(\kappa+\ell+1)}\int_0^\infty dx\, x^{2\ell-1}J_n^2(\beta x)\left(1+x^2\right)^{-(\kappa+\ell+1)}, \quad (21)$$

$$g_2 = (b)^{2\ell+2}\left(1+\frac{v_R^2}{\kappa\theta_\parallel^2}\right)^{-(\kappa+\ell+2)} \cdot \int_0^\infty dx\, x^{2\ell+1}J_n^2(\beta x)\left(1+x^2\right)^{-(\kappa+\ell+2)}, \quad (22)$$

$$b = \left\{\kappa\theta_\perp^2\left(1+\frac{v_R^2}{\kappa\theta_\parallel^2}\right)\right\}^{1/2}, \quad (23)$$

$$\beta = k_\perp b/\Omega_c. \quad (24)$$

A similar expression with some changes is obtained for distribution function equation (13)

$$D_i^\kappa = -\frac{2\pi^2\omega_{ph}^2}{k^2k_\parallel}\sum_{n=-\infty}^{\infty}\left[2\ell an\Omega_c g_1 - 2a(\kappa+1)\frac{n\Omega_c}{\kappa v_{th_\perp}^2}g_2 - 2a(\kappa+1)\frac{k_\parallel v_R}{\kappa v_{th_\parallel}^2}g_2\right], \quad (25)$$

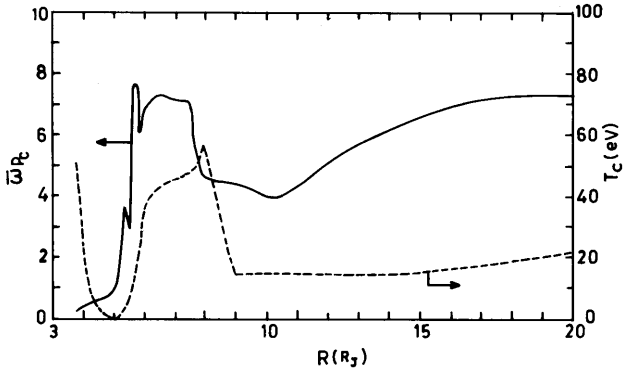

Figure 1. Variation of $\overline{\omega}_{pc}$ ($=\omega_{pc}/\Omega_c$) and the temperature of the thermal electron population, T_c, with radial distance in the magnetosphere of Jupiter at the magnetic equator.

where

$$a = \frac{\Gamma(\kappa+1)}{\pi^{3/2} v_{th_\perp}^2 v_{th_\parallel} \kappa^{\ell+3/2} \Gamma(\ell+1)\Gamma(\kappa-\ell-1/2)(v_{th_\perp})^{2\ell}}, \quad (26)$$

$$g_1 = (b)^{2\ell}\left(1+\frac{v_R^2}{\kappa v_{th_\parallel}^2}\right)^{-(\kappa+1)} \int_0^\infty dx\, x^{2\ell-1} J_n^2(\beta x)\left(1+x^2\right)^{-(\kappa+1)}, \quad (27)$$

$$g_2 = (b)^{2\ell+2}\left(1+\frac{v_R^2}{\kappa v_{th_\parallel}^2}\right)^{-(\kappa+2)} \int_0^\infty dx\, x^{2\ell+1} J_n^2(\beta x)\left(1+x^2\right)^{-(\kappa+2)}, \quad (28)$$

$$b = \left\{\kappa v_{th_\perp}^2\left(1+\frac{v_R^2}{\kappa v_{th_\parallel}^2}\right)\right\}^{1/2}. \quad (29)$$

In equation (4), D_i (**k**, ω_r) = $D_i^M + D_i^\kappa$.

[11] Using equation (15) and assuming $k_\parallel = 0$, we obtain

$$\frac{\partial D_r}{\partial \omega_r} = \frac{4\omega_r \omega_{pc}^2}{\lambda} \sum_{n=1}^{\infty} e^{-\lambda} I_n(\lambda) \frac{n^2}{\left(\omega_r^2 - n^2\Omega_c^2\right)^2}. \quad (30)$$

For finite $k_\parallel$, Bernstein modes are damped because of background thermal electron population, as is noted from equation (17). The error involved in using equation (15) with $k_\parallel = 0$ is of the order $v_c^2/2v_R^2$. We shall restrict $k_\parallel$ to values such that $v_c/v_R \leq 1/3$. This restriction is found to be consistent with damping calculated from equation (17).

3. Plasma Parameters for Jupiter's Magnetosphere

[12] A model of thermal plasma parameters of the Jovian magnetosphere based on various observations has been presented by *Divine and Garrett* [1983]. The model is based primarily on in situ data returned by experiments on the Pioneer and Voyager spacecrafts, supplemented by Earth-based observations and theoretical considerations. Time variations have been neglected in the model. Warm electrons are fitted with the kappa distribution function in which charge neutrality is not maintained. Values of the parameter κ for electrons are found to be about 2. In the cold (thermal) plasma model, all species are described by isotropic Maxwellian distributions having a common temperature. In the thermal plasma model the basic distance variable is Jovicentric distance r rather than L (this is equivalent to assuming that field lines are circles and dipole offset is negligible), and the plane of symmetry is the centrifugal equator. The model reproduces the various plasma features to within a factor of 2. The uncertainty may be large, perhaps a factor of 10, at large latitudes ($\lambda > 40°$) and at $r > 12\ R_J$ (for energies above several keV). We use this model to calculate electron number density and temperature. It may be pointed out that the model of *Divine and Garrett* [1983] underestimates the electron densities as measured during the Ulysses encounter [*Bird et al.*, 1992]. However, Ulysses measurements refer mainly to higher magnetic latitudes. In the present work we have utilized the *Divine and Garrett* [1983] model at magnetic equator, where the model predictions should be in agreement with the observations. Figure 1 shows the variation of $\overline{\omega}_{pc} = \omega_{pc}/\Omega_c$ and temperature T_c with radial distance at the magnetic equator (150°W, 6.6°S). An offset, tilted dipole is used to calculate the magnetic field. Figure 2 shows the typical electron distribution function for warm and energetic electrons [*Divine and Garrett*, 1983]. We have performed growth rate calculations at two representative radial distances at the magnetic equator (150°W, 6.6°S): (1) $R = 10\ R_J$, $\overline{\omega}_{pc} = 4$, $n_e = 30\ \text{cm}^{-3}$, and $T_c = 15$ eV and (2) $R = 7.4\ R_J$, $\overline{\omega}_{pc} = 7.1$, $n_e = 577\ \text{cm}^{-3}$, and $T_c = 47$ eV. Suprathermal number density n_h is assumed to be 1.4% of n_c, and $T_h = 4$ keV. R_J is the radius of Jupiter. Calculations are performed for spectral index $\kappa = 2, 3$ and loss cone index $\ell = 1, 2, 3$.

4. Results

[13] The variation of normalized temporal and spatial growth rates with η ($\omega_r/\Omega_c = n + \eta$) for electrostatic ECH

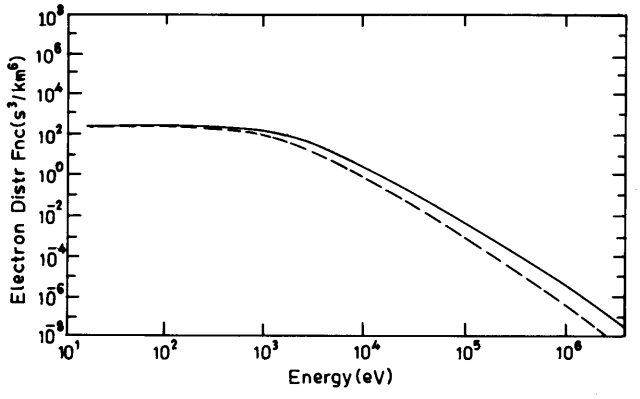

Figure 2. Sample distribution function for warm and energetic electrons for 6 R_J, 110°W, 0° latitude. Dashed line indicates observed values fitted with $\kappa = 2.32$; solid line indicates observed values fitted with $\kappa = 2$, $n_h = 0.014\ n_c$, and $T_h = 4$ keV.

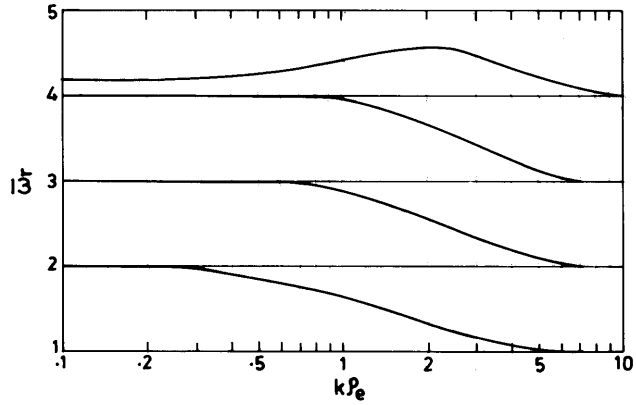

Figure 3. Dispersion relation for electron cyclotron harmonic (ECH) emissions at radial distance $R = 10\ R_J$.

instability for various values of κ, ℓ, ψ, T_h, and n_{ce} and other fixed values of plasma parameters are shown (see Figures 4 and 6–13). The choice of particle distribution function modifies the solution of electrostatic ECH growth relation. This aspect is demonstrated in this section. A direct comparison is made between the results for *Summers and Thorne* [1991, 1995] and *Leubner and Schupfer* [2001] distributions.

4.1. Results for ST Model Distribution Function (Equation (8))

[14] Dispersion relations for $R = 10\ R_J$ are shown in Figure 3, and temporal growth rates for ECH bands first, second, and third are shown in Figure 4 for $\psi = 89°$, 87°, and 85° using $\kappa = 2$ and $\ell = 1$. It is noted that the damping increases faster for higher harmonics as ψ decreases. Thus the second and third harmonics have disappeared at 85°. The behavior of growth rate strongly depends on the parameter β, which appears in the integrals g_1 and g_2. The integrals for $\ell = 1$ which appear in growth rate are shown in Figure 5, where I is given by

$$I = \int_0^\infty dx\, x J_n^2(\beta x)\left(1 + x^2\right)^{-(N+2)}. \tag{31}$$

Parameter β depends on the ratio $v_R/\theta_\parallel$. For $v_c/v_R \le 1/3$, $v_R/\theta_\parallel \ge 3v_c/\theta_\parallel$. For small $v_R/\theta_\parallel$, $\beta \approx \rho_e k\theta_\parallel/v_c$; ρ_e is gyroradius ($=v_c/\Omega_c$). For large $v_R/\theta_\parallel$, β approaches $(\overline{\omega}_r - n)/\cos\psi$, which is the same as for power law ($\overline{\omega}_r = \omega_r/\Omega_c$). In this case, $\beta \ge 3\rho_e k$. The location and magnitude of the peak in Figure 4 depend on the variation of I with β as shown in Figure 5. The integrals appearing in equation (31) have been carried out using asymptotic expressions given by *Barbosa and Kurth* [1980] and *Summers et al.* [1994]. For smaller values of β, integrals are carried out numerically. Figure 6 shows the temporal growth rates for ECH bands at a radial distance of 7.4 R_J for $\kappa = 2$ and $\ell = 1$. Comparing Figure 6 with Figure 4, it is noted that the frequencies within each band shift toward lower values at $R = 7.4\ R_J$ compared with values at $R = 10\ R_J$. This is due to the lower value of T_c (15 eV) at $R = 10\ R_J$ compared with the value 47 eV at $R = 7.4\ R_J$. We further

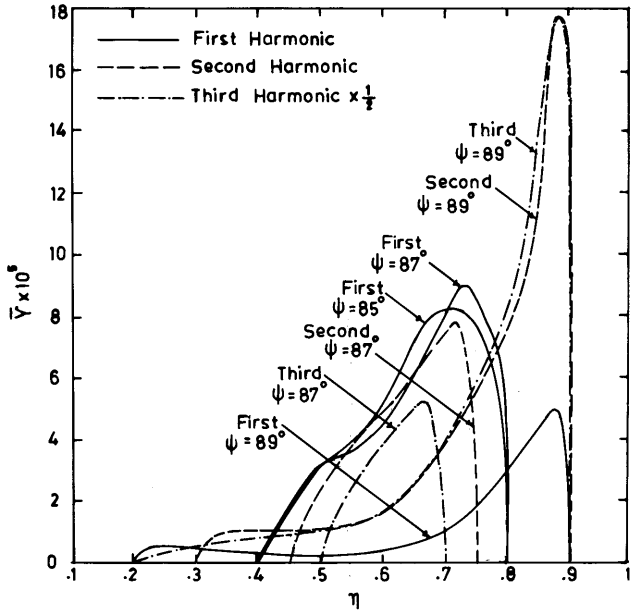

Figure 4. Normalized temporal growth rates $\overline{\gamma}$ ($=\gamma/\Omega_c$) of ECH bands at radial distance $R = 10\ R_J$ for $\kappa = 2$ and $\ell = 1$. The frequency within each band is $\overline{\omega}_r$ ($=\omega_r/\Omega_c$) $= n + \eta$, where $n = 1, 2, 3$ and η lies between 0 and 1 (*Summers and Thorne* [1991, 1995] model).

note that the fourth harmonic band has been totally damped at $\psi = 87°$ and the second harmonic band is damped at $\psi = 85°$. Also, the bandwidth of each harmonic band decreases as ψ is decreased. It may also be seen from Figures 4 and 6 that the growth of waves is, in general, higher at $R = 10\ R_J$ compared with the

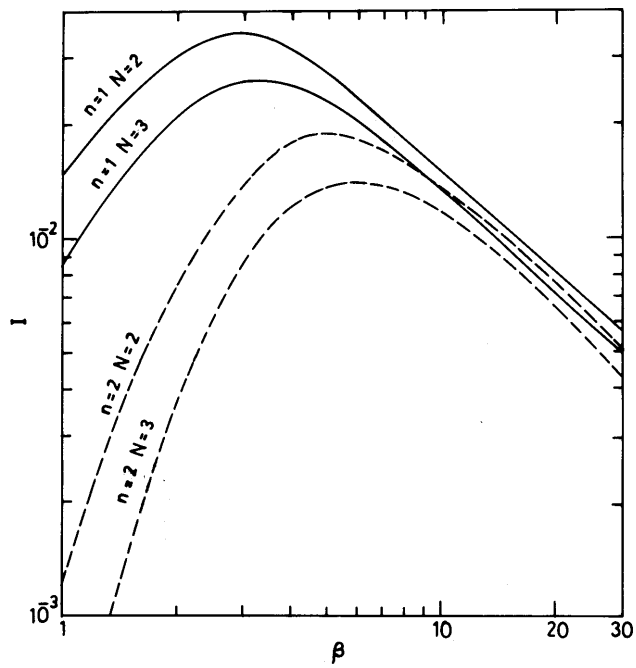

Figure 5. Variation of integrals I (equation (31)) with parameter β.

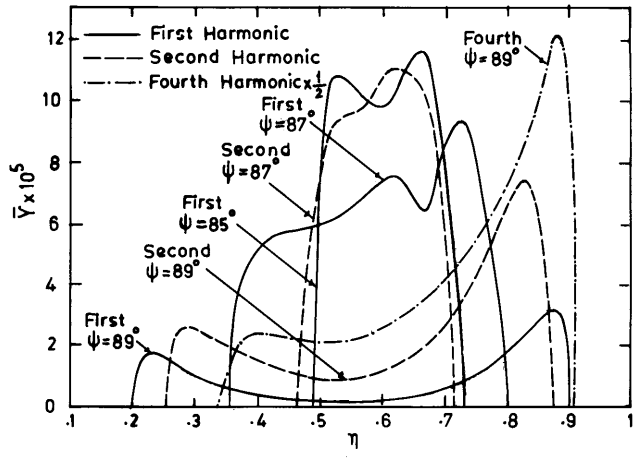

Figure 6. Same as Figure 4 but for $R = 7.4\ R_J$ (ST model).

values at $R = 7.4\ R_J$. Thus the frequency of ECH emission is a diagnostic parameter for the temperature of thermal electron population in the magnetosphere of Jupiter. *Barbosa and Kurth* [1980] calculated the temporal growth rates for ECH bands for first and second harmonic bands using power law distribution function using the parameters $n_e = 100\ \mathrm{cm}^{-3}$, $T_c = 100$ eV, and $\overline{\omega}_{pc} = 4$. These parameters are closer to our values of $R = 7.4\ R_J$. Barbosa and Kurth find the peak growth rate at the same value of η for both harmonics and almost the same growth rates for both harmonics. Comparing these values with Figure 6, we find that in our case at $\psi = 89°$, the peak growth rate of the second harmonic is larger than its value for the first harmonic. At $\psi = 87°$ the growth rates are also same for both harmonics. The location of peak in our cases is at a larger value of η compared to *Barbosa and Kurth* [1980]. This is consistent with our finding that the peak shifts to lower η for higher values of T_c. In Figure 7 we show the convective growth rate $k_i = -\gamma/V_g$ for ECH bands at $R = 10\ R_J$, where V_g is the group velocity. From Figure 3 it is noted that the group velocity of the waves within a band decreases with decrease in frequency. This effect is reflected in Figure 7.

4.1.1. Variation of κ and ℓ

[15] In Figure 8 we show the growth rates at $R = 7.4\ R_J$ using $\kappa = 3$ and $\ell = 1$. Comparing with growth rates for $\kappa = 2$ and $\ell = 1$ (Figure 6), we note that at $\psi = 89°$ the first and second harmonic bands are slightly enhanced while the fourth harmonic band is reduced. At $\psi = 87°$ (not shown) and $\psi = 85°$ the growth rates for $\kappa = 3$ and $\ell = 1$ are slightly reduced compared with values for $\kappa = 2$ and $\ell = 1$. The slight enhancement in first and second harmonic bands at $\psi = 89°$ is due to the fact that the decrease in coefficient "a" is more than compensated by the increase in g_1 and g_2 (equations (20)–(22)). Figure 9 shows the growth rates at $R = 7.4\ R_J$ using $\kappa = 2$ and $\ell = 3$. It is noted that the

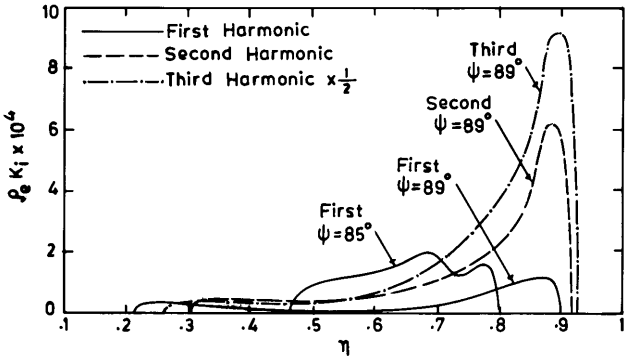

Figure 7. Normalized convective growth rates of ECH bands at $R = 10\ R_J$ for $\kappa = 2$ and $\ell = 1$ (ST model).

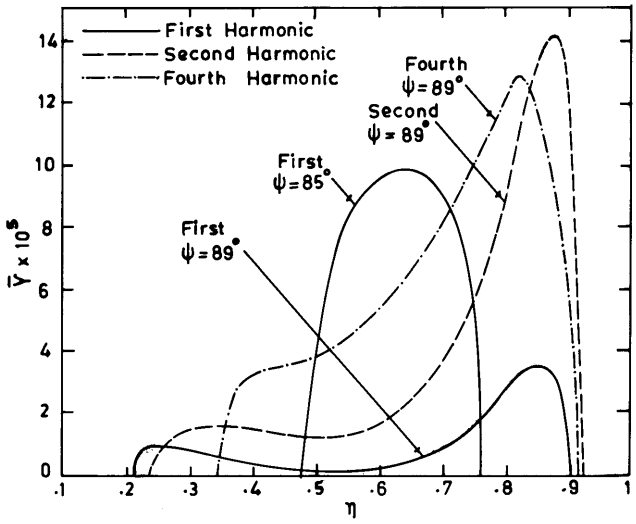

Figure 8. Normalized temporal growth rate of ECH bands at radial distance $R = 7.4\ R_J$ for $\kappa = 3$ and $\ell = 1$ (ST model).

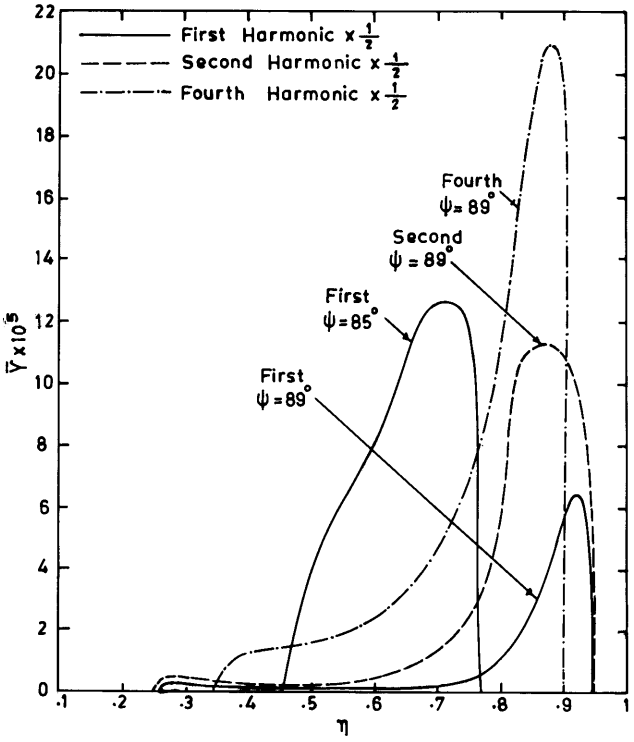

Figure 9. Same as Figure 8 but for $\kappa = 2$ and $\ell = 3$ (ST model).

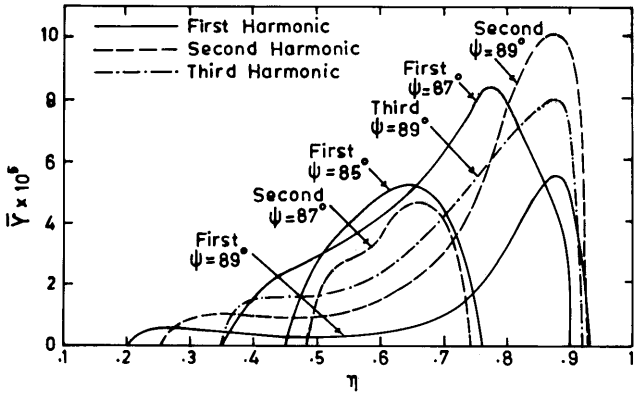

Figure 10. Same as Figure 4 but for $n_{ce} = 90$ cm^{-3} (3 times value used in Figure 4) (ST model).

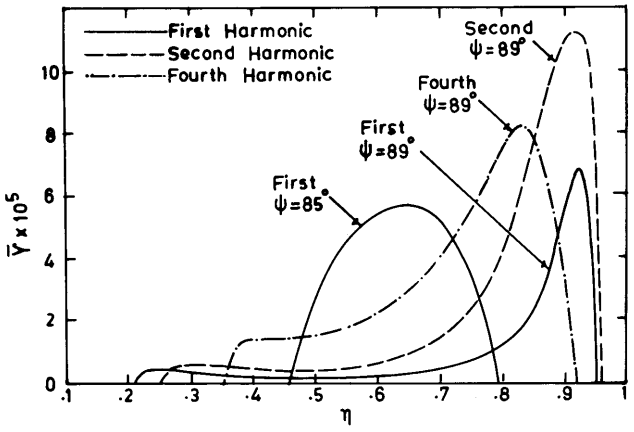

Figure 12. Same as Figure 11 but for $\kappa = 3$ and $\ell = 1$ (LS model).

growth rates are considerably larger (almost a factor of 2) compared with values for $\kappa = 2$ and $\ell = 1$ (Figure 6).

4.1.2. Variation of T_h

[16] A case study was performed to study the effect of T_h (equations (8)–(10)) on growth rate at $R = 10\ R_J$. While no systematic changes were noted, two points may be mentioned. First, as T_h is changed from 2 keV to 6 keV, the growth for second and third ECH bands decreases at $\psi = 87°$ and 85°. Second, at $\psi = 89°$, growth increases for first ECH bands as T_h increases. However, the third harmonic band, which in this case is near UHR, is always the most intense band, which is in accord with observations.

4.1.3. Variation of n_{ce} (Cold Electron Density)

[17] It has been noted in section 3 that the *Divine and Garrett* [1983] model underestimates the thermal electron density outside the Io torus. We have therefore made a study of growth rates for $R = 10\ R_J$, $\kappa = 2$, and $\ell = 1$ using $n_{ce} = 90$ cm^{-3}, which is 3 times the value used in Figure 4. Dispersion relation and growth rates have been calculated. Growth rates are shown in Figure 10. It is noted that the growth rates are generally considerably smaller than the values shown in Figure 4. Comparing these with growth rates shown in Figure 6 ($R = 7.4\ R_J$), it is found that the values at $R = 10\ R_J$ are, in general, smaller than the values of $R = 7.4\ R_J$, which is in better agreement with observations [*Kurth et al.*, 1980; *Kurth*, 1992].

4.2. Results for LS Model Distribution Function (Equation (13))

[18] In Figure 11 we show the growth rates (equation (25)) at $R = 7.4\ R_J$ using the distribution function equation (13) given by *Leubner and Schupfer* [2001] with $\kappa = 2$ and $\ell = 1$. It may be noted that the first harmonic band at $\psi = 89°$ is more intense compared with second and fourth bands. However, in Figure 6 the fourth band is more intense than the first and second bands. In Figure 12 we show the growth rates for $\kappa = 3$ and $\ell = 1$ for the same radial distance. It is noted that the growth rates are considerably increased. Finally, in Figure 13 we show the effect of changing "ℓ" on growth rates using $\kappa = 3$ and $\ell = 2$. It is noted that the growth rates are considerably reduced compared with values shown in Figure 11. This is mainly due to the reduction in the coefficient $ab^{2\ell}$ appearing in equations (25), (26), and (29).

5. Discussion and Conclusions

[19] Our calculations for distribution function equation (8) show that the first ECH band remains undamped up to about $\psi = 85°$, and the higher bands start damping at $\psi \leq$

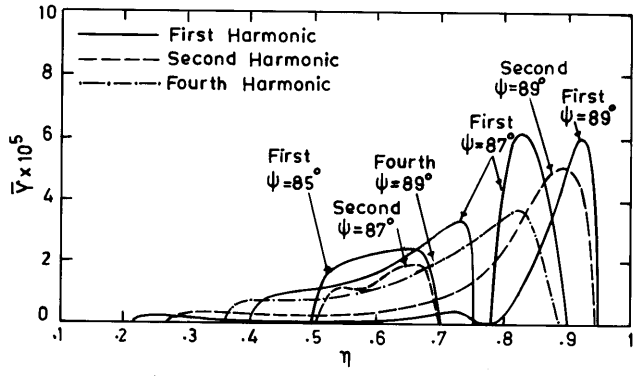

Figure 11. Normalized temporal growth rate of ECH bands at radial distance $R = 7.4\ R_J$ for $\kappa = 2$ and $\ell = 1$ (*Leubner and Schupfer* [2001] model).

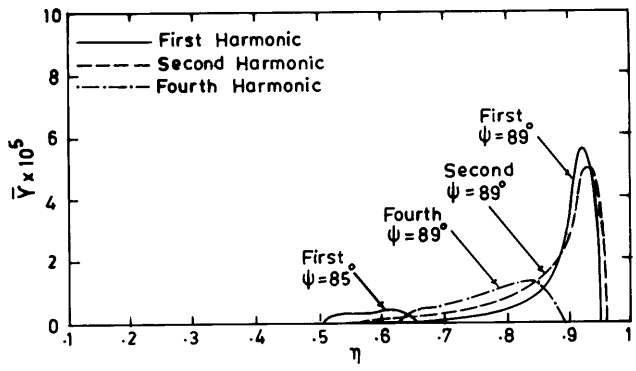

Figure 13. Same as Figure 11 but for $\kappa = 3$ and $\ell = 2$ (LS model).

87°. This may account for the observation [*Kurth et al.*, 1980; *Stone et al.*, 1992; *Gurnett et al.*, 1996a] that the first harmonic band is the main band that is generally observed. Next, the observations show that the band near upper hybrid resonance is usually very intense. This is also in agreement with our calculations, as can be seen in Figures 4, 6, 8, and 9, where the third band in Figure 4 ($\overline{\omega}_{pc} = 4$) is very strong and the fourth band in Figures 6, 8, and 9 ($\overline{\omega}_{pc} = 7$) is also very strong. We also find that the frequency within the band shifts to a lower value as the thermal temperature T_c is increased. However, this cannot be verified because of a lack of observational data. Comparing Figure 4 ($R = 10\ R_J$) and Figure 6 ($R = 7.4\ R_J$), we note that the intensity of first band at $\psi = 85°$ decreases as radial distance is increased. However, for other bands and for other values of ψ, growths do not decrease as radial distance is increased. This is not in accord with observations. This is due to the inadequacy of plasma parameters used in the model as pointed out in section 4.1.3.

[20] Using the distribution function equation (13), it is noted from Figure 11 that for $\kappa = 2$ and $\ell = 1$ at $R = 7.4\ R_J$ the first harmonic is the most intense band in comparison with second and fourth ECH bands. This is in better accord with observation compared with the results for distribution function equation (8) (refer to Figure 6). However, the results for variation of κ and ℓ are quite different in this case compared with the case for equation (8).

[21] We have thus made a comprehensive study of electron cyclotron harmonics emissions using kappa loss cone distribution function in the magnetosphere of Jupiter. Two types of electron distribution functions representing suprathermal tails have been used, one given by *Summers and Thorne* [1995] and the other given by *Leubner and Schupfer* [2001]. In the latter case the amplitudes of ECH bands decrease as the loss cone index ℓ is increased, while in the former the reverse is the case. It is found that the first harmonic band remains undamped for lower values of ψ ($\psi = 85°$), compared with higher bands, which are damped for $\psi \leq 87°$ and $\psi \leq 89°$. Thus the first ECH band can be seen in a larger cone (semicone angle of 5°) as compared with higher bands, for which the semicone angle is $\sim 1°-3°$. It is also noted that the bandwidth decreases as ψ is decreased from 89° to 85°. The observed fluctuation of amplitudes of ECH bands on a timescale of few seconds may be due to the change in the loss cone index ℓ of the suprathermal particle population. It is also found that the amplitudes of bands decrease with increasing radial distance when a higher value of thermal electron density is used at $R = 10\ R_J$ than that given by the *Divine and Garrett* [1983] model. This is in agreement with the Ulysses observation of thermal electron density outside the Io plasma torus. Thus the *Divine and Garrett* [1983] model is not consistent with observations of plasma waves outside the Io plasma torus. The present calculations are more detailed in comparison with the studies performed by *Barbosa and Kurth* [1980]. Plasma waves play an important role in Jovian auroral energetics. There is evidence that a part of the Jovian aurora is connected to the Jovian inner magnetosphere ($R < 12\ R_J$) [*Dols et al.*, 1992; *Clarke et al.*, 1994]. ECH waves can cause both energy diffusion and pitch angle scattering of keV electrons, leading to a precipitation of particles into the atmosphere. Scattering properties depend on the wave amplitudes [*Thorne*, 1983]. Present studies should be helpful in making estimates on scattering properties of ECH waves and thus contribute to a better understanding of the Jovian aurora.

[22] **Acknowledgments.** This work was supported by a research associateship award to one of the authors (A.K.T.) by the Council of Scientific and Industrial Research, Government of India. Calculations reported in the present work were carried out at the Computer Centre, Banaras Hindu University.

[23] **Editor's Acknowledgments.** Arthur Richmond thanks Michael Collier, Manfred P. Leubner, and another reviewer for their assistance in evaluating this manuscript.

References

Abramowitz, M., and I. A. Stegun (Eds.) (1970), *Handbook of Mathematical Functions With Formulas, Graphs, and Mathematical Tables*, U.S. Gov. Print. Off., Washington, D. C.

Barbosa, D. D., and W. S. Kurth (1980), Superthermal electrons and Bernstein waves in Jupiter's inner magnetosphere, *J. Geophys. Res.*, *85*, 6729–6742.

Belcher, J. W. (1983), The low energy plasma in the Jovian magnetosphere, in *Physics of the Jovian Magnetosphere*, edited by. A. J. Dessler, pp. 68–105, Cambridge Univ. Press, New York.

Bird, M. K., S. W. Asmar, J. P. Brenkle, P. Edenhofer, O. Funke, M. Patzold, and H. Volland (1992), Ulysses radio occultation observations of the Io plasma torus during the Jupiter encounter, *Science*, *257*, 1531–1535.

Bridge, H. S., et al. (1979a), Plasma observations near Jupiter: Initial results from Voyager 1, *Science*, *204*, 987–991.

Bridge, H. S., et al. (1979b), Plasma observations near Jupiter: Initial results from Voyager 2, *Science*, *206*, 972–976.

Clarke, J. T., L. Ben Jaffel, A. Vidal-Madjar, G. R. Gladstone, J. H. Waite Jr., R. Prange, J.-C. Gerard, J. Ajello, and G. James (1994), Goddard high-resolution spectrograph H_2 rotational spectra of Jupiter's aurora, *Astrophys. J.*, *430*, L73–L76.

Clemmow, P. C., and J. P. Dougherty (1969), *Electrodynamics of Particles and Plasmas*, 457 pp., Addison-Wesley, Boston, Mass.

Collier, M. R. (2004), Are magnetospheric suprathermal particle distributions (κ functions) inconsistent with maximum entropy considerations?, *Adv. Space Res.*, *33*, 2108–2112.

Divine, N., and H. B. Garrett (1983), Charged particle distributions in Jupiter's magnetosphere, *J. Geophys. Res.*, *88*, 6889–6903.

Dols, V., J. C. Gerard, F. Paresce, R. Prange, and A. Vidal-Madjar (1992), Ultraviolet imaging of the Jovian aurora with the Hubble Space Telescope, *Geophys. Res. Lett.*, *19*, 1803–1806.

Gurnett, D. A., and F. L. Scarf (1983), Plasma waves in the Jovian magntosphere, in *Physics of the Jovian Magnetosphere*, edited by A. J. Dessler, pp. 285–316, Cambridge Univ. Press, New York.

Gurnett, D. A., W. S. Kurth, A. Roux, S. J. Bolten, and C. F. Kennel (1996a), Galileo plasma wave observations in the Io plasma torus and near Io, *Science*, *274*, 391–392.

Gurnett, D. A., W. S. Kurth, A. Roux, S. J. Bolten, and C. F. Kennel (1996b), Evidence for a magnetosphere at Ganymede from plasma-wave observations by the Galileo spacecraft, *Nature*, *384*, 535–537.

Kurth, W. S. (1992), Comparative observations at plasma waves at the outer planets, *Adv. Space Res.*, *12*, 83–90.

Kurth, W. S., and D. A. Gurnett (1991), Plasma waves in planetary magnetospheres, *J. Geophys. Res.*, *96*, 18,977–18,991.

Kurth, W. S., D. D. Barbosa, D. A. Gurnett, and F. L. Scarf (1980), Electrostatic waves in the Jovian magnetosphere, *Geophys. Res. Lett.*, *7*, 57–60.

Kurth, W. S., D. A. Gurnett, A. M. Persoon, A. Roux, S. J. Bolton, and C. J. Alexander (2001), The plasma wave environment of Europa, *Planet. Space Sci.*, *49*, 345–363.

Leubner, M. P. (1982), On Jupiter's whistler emission, *J. Geophys. Res.*, *87*, 6335–6338.

Leubner, M. P. (2004), Core-halo distribution functions: A natural equilibrium state in generalized thermodynamics, *Astrophys. J.*, *604*, 469–478.

Leubner, M. P., and N. Schupfer (2001), A general kinetic mirror instability criterion for space applications, *J. Geophys. Res.*, *106*, 12,993–12,998.

Mace, R. L. (1998), Whistler instability enhanced by suprathermal electrons within the Earth's foreshock, *J. Geophys. Res.*, *103*, 14,643–14,654.

Mathews, J., and R. L. Walker (1965), *Mathematical Methods of Physics*, Benjamin, White Plains, New York.

Scarf, F. L., D. A. Gurnett, and W. S. Kurth (1981), Measurements of plasma wave spectra in Jupiter's magntosphere, *J. Geophys. Res.*, *86*, 8181–8198.

Stone, R. G., et al. (1992), Ulysses radio and plasma waves observations in the Jupiter environment, *Science*, *257*, 1524–1531.
Summers, D., and R. M. Thorne (1991), The modified plasma dispersions function, *Phys. Fluids B*, *3*, 1835–1847.
Summers, D., and R. M. Thorne (1992), A new tool for analysing microinstabilities in space plasmas modelled by a generalized Lorentzian (kappa) distribution, *J. Geophys. Res.*, *97*, 16,827–16,832.
Summers, D., and R. M. Thorne (1995), Plasma microinstabilities driven by loss-cone distributions, *J. Plasma Phys.*, *53*, 293–315.
Summers, D., S. Xue, and R. M. Thorne (1994), Calculation of the dielectric tensor for a generalized lorentzian (kappa) distribution function, *Phys. Plasmas*, *1*, 2012–2025.
Thorne, R. M. (1983), Microscopic plasma processes in the Jovian magnetosphere, in *Physics of the Jovian Magnetosphere*, edited by A. J. Dessler, pp. 454–488, Cambridge Univ. Press, New York.
Zarka, P. (2004), Radio and plasma waves at the outer planets, *Adv. Space. Res.*, *33*, 2045–2060.

R. P. Singhal and A. K. Tripathi, Department of Applied Physics, Institute of Technology, Banaras Hindu University, Varanasi 221005, Uttar Pradesh, India. (rpsinghal@bhu.ac.in; aktrip2001@yahoo.co.in)